Springer

Journal of
Mechanical
Science and
Technology

Journal of Mechanical Science and Technology 22 (2008) 1174~1180

www.springerlink.com/content/1738-494x

Numerically analyzed supersonic flow structure behind the exit of a two-dimensional micro nozzle

Sungcho Kim[1,*], Jeong Soo Kim[1], Jongwook Choi[1], Jeong Park[2] and Soon Duk Kwon[3]

[1]*School of Mechanical & Aerospace Engineering, Sunchon National University, 315 Maegok-dong, Suncheon, Jeonnam, 540-742, Korea*

[2]*Division of Mechanical Engineering, Pukyong National University, San 100, Yongdang-dong, Nam-gu, Busan, 608-739, Korea*

[3]*Department of Mechanical Engineering, Graduate School, Sunchon National University, 315 Maegok-dong, Suncheon, Jeonnam, 540-742, Korea.*

(Manuscript Received January 9, 2007; Revised November 13, 2007; Accepted April 4, 2008)

Abstract

The compressible flow field is numerically analyzed in a two-dimensional converging-diverging nozzle of which the area ratio, exit to throat, is 1.8. The solver is FLUENT and the embedded RNG $k-\varepsilon$ model is adopted to simulate turbulent flow. The plume characteristics such as shock-cell structure are discussed when nozzle pressure ratio and stagnation temperature at the nozzle entrance are varied. The downstream flow field can be classified into two types based on the shock shapes generated near the nozzle exit. First, a reiterative pattern in the plume is not formed between the slip streams in case that a strong lambda-type shock wave exists. Second, when oblique shock waves are crossing each other on the nozzle centerline, a shock cell structure appears in the plume field. Even when the flow field is changed due to stagnation temperature, the upstream of the shock wave is little affected. Especially, the pressure distributions on the nozzle centerline behind the shock wave are rarely influenced by the stagnation temperature, that is, the product of density and temperature is nearly constant provided that the working fluid is a perfect gas. Therefore, the pressure field shows quasi-isobaric behavior far downstream.

Keywords: Nozzle pressure ratio (NPR); Plume structure; RNG $k-\varepsilon$ turbulence model; Shock cell; Mach reflection, Regular reflection

1. Introduction

A converging-diverging nozzle is used to make supersonic flow, of which the field should be analyzed in detail to predict its performance like thrust, etc. The supersonic flow inside a nozzle is adjusted by interacting with ambient condition through the subsonic boundary layer in a nozzle [1]. It is very essential in designing small thrusters used for the attitude control of satellites to look into the physical phenomenon of a plume minutely. That is, the flow properties like pressure, density, temperature and velocity distributions should be closely examined in order to find the flow characteristics in accordance with variations of nozzle geometry or pressure ratio. Even though the primary operating environment of satellite thrusters is vacuous in space, the pressure ratio between entrance and exit of a nozzle is also of importance, and the fundamental analysis for thruster performance is useful. Therefore the analysis using the Navier-Stokes equations based on continuum mechanics is reasonable to verify the basic flow characteristics of a thruster nozzle. Koo [2] inquired into the effects of the injector nozzle geometry and the operating pressure conditions such as opening, ambient, and injection pressures on the transient fuel spray behavior. Aoki et al. [3] experimentally investigated the influence of the nozzle lip thickness on the supersonic jet screech tone, and described that it is strongly dependent on whether the jet flow at

*Corresponding author. Tel.: +82 61 750 3534, Fax.: +82 61 750 3530
E-mail address: ksc@sunchon.ac.kr
DOI 10.1007/s12206-008-0405-x

the nozzle exit is over-expended or under-expanded. Han [4] suggested that the $k-\varepsilon$ turbulence model was reasonable to solve supersonic jets even where the boundary layer swirl existed at the nozzle exit.

In this paper, the plume structure is examined when NPR (nozzle pressure ratio) is changed. And the effect of the stagnation temperature at the nozzle entrance on the flow structure is investigated.

2. Computational work

The nozzle geometry in Fig. 1 is designed to be identical to one in the reference [5]. It is a symmetric two-dimensional converging-diverging nozzle, and the area ratio of the exit to the throat (0.541 in. wide) is 1.8. The multi-block grid system is generated by quads only, and the grid dependence was numerically experimented by using several grid densities to capture the shock waves successfully. Many computational experiments were carried out with varying the size of computational domain and the grid quality. And then the most optimal grid system was chosen to describe the detailed properties of flow like weak shocks. The grid is sufficiently dense near the nozzle inside wall to realize the viscous sublayer. More information for the grids and the boundary conditions is described by Kwon et al. [6].

The two-dimensional steady non-reactive viscous compressible flow is solved numerically when the working fluid is air. The governing equations are given in (1) to (4), which are the continuity equation, the momentum conservation equation (Navier-Stokes equations), the energy conservation equation, and the equation of state, respectively:

$$\frac{\partial}{\partial x_i}(\rho u_i) = 0 \tag{1}$$

$$\frac{\partial}{\partial x_i}(\rho u_i u_j) = -\frac{\partial p}{\partial x_i} + \frac{\partial \tau_{ij}}{\partial x_i} \tag{2}$$

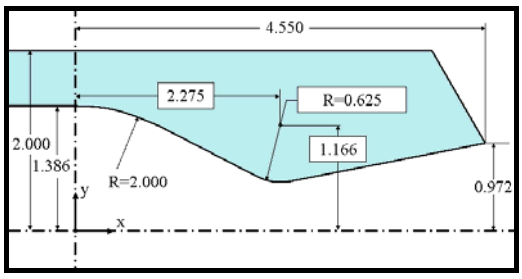

Fig. 1. Dimension of the two-dimensional nozzle (Unit: inch).

$$\frac{\partial \rho e u_i}{\partial x_i} = -\frac{\partial p u_i}{\partial x_i} + \frac{\partial (u_j \tau_{ij} - q_i)}{\partial x_i} \tag{3}$$

$$p = \rho RT \tag{4}$$

After the turbulence models embedded in FLUENT are tested, the RNG k-ε model is adopted to deal with the turbulent flow. And the model equations are briefly described as follows:

$$\frac{\partial \rho k u_i}{\partial x_i} = \frac{\partial}{\partial x_j}\left(\alpha_k \mu_{eff} \frac{\partial k}{\partial x_j}\right) + \mu_t S^2 - \rho\varepsilon\left(1 - 2\sqrt{\frac{k}{a^2}}\right) \tag{5}$$

$$\frac{\partial \rho \varepsilon u_i}{\partial x_i} = \frac{\partial}{\partial x_j}\left(\alpha_\varepsilon \mu_{eff} \frac{\partial \varepsilon}{\partial x_j}\right) + C_{1\varepsilon}\frac{\varepsilon}{k}\mu_t S^2 - \rho\frac{\varepsilon^2}{k}\left(C_{2\varepsilon} + \frac{C_\mu \rho \eta^3 (1-\eta/\eta_0)}{1+\beta\eta^3}\right) \tag{6}$$

$$\mu_t = \rho C_\mu k^2 \varepsilon^{-1} \tag{7}$$

The Sutherland law is used to calculate the absolute viscosity depending on temperature. The second order upwind scheme is applied for the spatial discretization. The details on the numerical procedure are mentioned in the reference [7]. The stagnation conditions are prescribed at the nozzle entrance, and chosen to match the experiments. The various ratios of stagnation pressure to atmospheric pressure, i.e., NPR= 1.2~9, are applied for the flow to be accelerated in the nozzle, and also the corresponding stagnation temperatures are evaluated through the equation of state for air. Outer far boundaries are established as the standard atmosphere condition, and the no-slip and adiabatic conditions are given at all the solid walls.

3. Computational results and discussions

3.1 Pressure field

Normalized static pressure (p/p_s) distributions on the inside nozzle wall are presented in Fig. 2, where x is the coordinate of the main flow direction along the nozzle centerline and x_t denotes the distance between the nozzle entrance and the nozzle throat. The pressure discrepancies between the present calculation and the experiments [5] are less than 5%, and the computations become more accurate as NPR increases. Some differences near the throat at low NPRs around 1.255-1.808 are supposed to be related to the turbulence model. That is, the flow field is computed as if a shock wave is generated near the wall of the throat because the RNG $k-\varepsilon$ model is pertinent to

analysis of a high Reynolds number flow. The pressure near the nozzle throat is distributed in an irregular wave pattern; however, in cases of almost NPRs the static pressure drops in similar trend. The irregularity is due to the characteristics in the grid distribution such as the kind of a tolerance problem which might occur in the process of the grid generation. The geometric gradients (dy/dx) between adjacent grid points on the nozzle inside wall and the static pressure at NPR=8.945 are shown together in Fig. 3 for the purpose of closely investigating why pressure drops in irregular wavelike behavior. The shape near the nozzle throat and the starting region of the converging part are curves, but the rest are straight lines. The geometric gradients on the curved nozzle surface, i.e., near the throat, discontinuously change. Namely, concave and convex surfaces (or corners) locally exist from the microscopic point of view; therefore, compression and expansion waves could originate in the corresponding corners if the flow is supersonic. However, this does not hold near the nozzle throat since flow is not purely supersonic. In the front region less than x/x_t =0.4, the geometric gradient does not have any influence on the pressure distribution, i.e., no irregular pattern in the pressure distribution occurs, since flow is completely subsonic. The detailed explanation could be found in the reference [6].

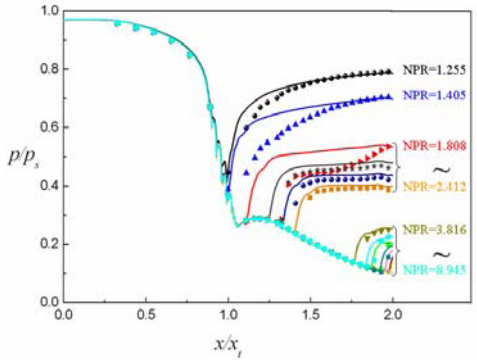

Fig. 2. Static pressure distribution on the wall (lines: com putation, symbols: experiment [5]).

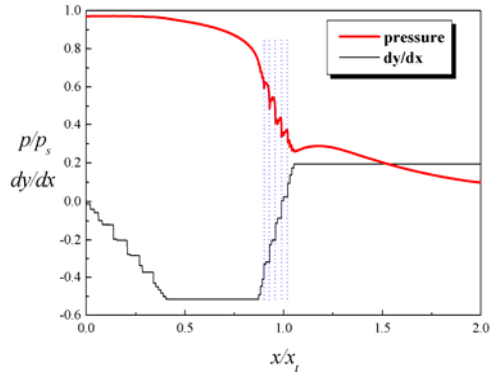

Fig. 3. Relationship between the static pressure distribution and the geometric gradient of the wall surface (NPR=8.945).

3.2 Plume structure

For the various pressure ratios (NPRs), the Mach number distributions on the nozzle centerline are drawn in Fig. 4, where the coordinate of the nozzle centerline is nondimensionalized by the length of the divergent part (L_S). So x/L_S =0, 1 and 2 denote the locations of the entrance, throat and exit of the nozzle, respectively. The Mach numbers at all NPRs change in the same way until they reach their peak values. As NPR increases, the overall Mach number distribution increases rightly, but they differently change according to NPR by interaction with ambient conditions. In cases of NPR= 1.255 and 1.405, whole flow fields become subsonic, and thus flows are not choked. The flow accelerated in a nozzle is decelerated to be adapted to the recovered pressure. The Mach number is partially constant in the range of x/L_s =2～5.5 because of the flow inertia. And the speed of flow gradually reduces to the free stream velocity (quiescent there) by momentum diffusion. The nozzle flow is choked at NPRs above 1.608. When the NPRs range is from 1.608 to 2.607, flow is accelerated to the supersonic speed, and a normal shock wave is generated to fit the outer boundary condition. The flow field behind the shock wave is similar to the subsonic case. When NPRs are 3.014 and 3.413, the size of a normal shock wave decreases relatively and the intensity of the reflected shock wave grows. The weak cell structure appears for a short while and then disappears behind a normal shock wave because of the shock wave reflection. Likewise, the subsequent flow slows down to the free stream velocity as subsonic flow does.

The Mach number distributions on the nozzle centerline are shown in Fig. 5 after extracting the cases of NPR=3.816 and 4.217 from Fig. 4. The flow speed increases up to the supersonic state. Oblique shock waves separated from both sides of the nozzle walls are crossing each other on the nozzle centerline. The cross section of oblique shock waves at NPR=3.816 is redrawn in the bottom box of Fig. 5. The crossing of oblique shock waves at the nozzle centerline is from

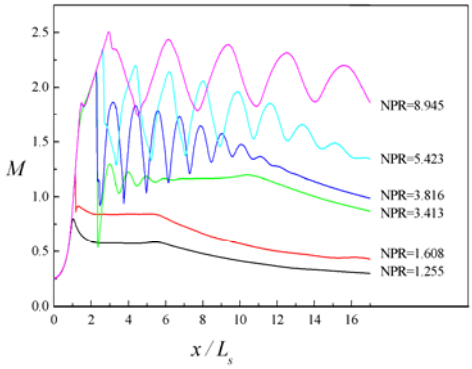

Fig. 4. Mach number distributions along the nozzle centerline at the various pressure ratios.

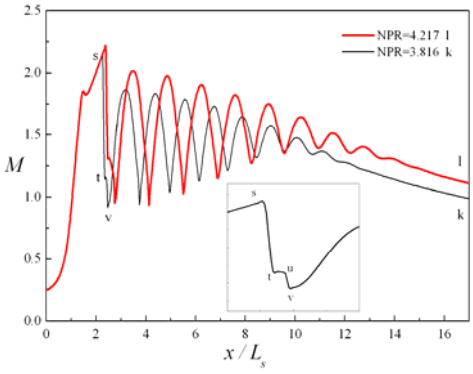

Fig. 5. Mach number distributions along the nozzle centerline when supersonic flow with the weak cell structure is developed behind the crossed oblique shock waves.

point (s) to point (t) as shown in Figs. 5 and 6. Immediately after shock waves are crossed the Mach number is more than 1 as yet, unlike the cases of NPRs of 3.014 and 3.413. A weak normal shock wave is generated behind the oblique shocks' crossing (Fig. 6). It originates from the points where two different oblique shock waves meet each other. And that confirms the phenomenon from point (u) to point (v) in Figs. 5 and 6. When NPRs are in the range from 4.620 to 7.030, oblique shock waves are also crossed on the nozzle centerline and the strong cell structure comes out in a plume. The size and intensity of the cell dwindle in proportion to the streamwise cell scale. Based on the Mach number distributions on the nozzle centerline in Fig. 4, the flow at NPR=8.945 is fully developed and close to the design condition of the nozzle. Fig. 7 illustrates the Mach number contours of the representative cases which are discussed previously. When NPR is from 5.018 to 8.945, a clear cat's-eye type cell

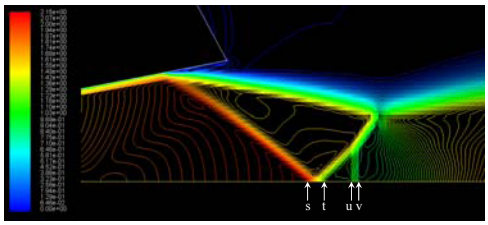

Fig. 6. Mach number contours at NPR=3.816 (The four locations, s, t, u and v correspond to them in Fig. 5.).

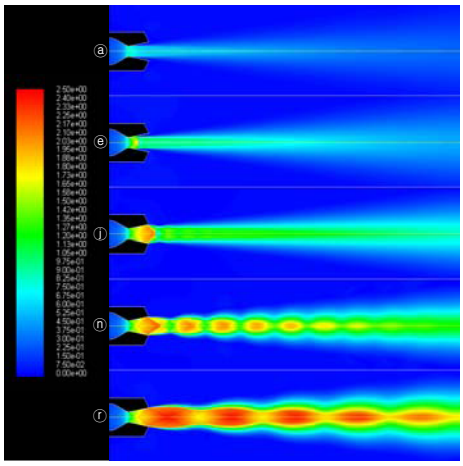

Fig. 7. Two-dimensional Mach number distributions at the various pressure ratios (The NPRs of ⓐ, ⓔ, ⓙ, ⓝ, ⓡ are 1.255, 2.008, 3.413, 5.018, 8.945, respectively).

structures occur, that is, the exhausted flow from the nozzle exit is thought to be a kind of the virtual nozzle flow. This is verified also in Figs. 4 and 5 where the Mach numbers distribute more or less periodically.

3.3 The effects of the stagnation temperature variation on the flow characteristics

When the stagnation temperature changes at the fixed NPR (3.413), i.e., 500, 1000 and 2000K, the Mach number distributions on the nozzle centerline are shown in Fig. 8. The stagnation temperature given at the nozzle entrance scarcely influenced the Mach number distributions upstream of a normal shock wave, but the Mach number distributions at the section of shock cells are a little different due to the change of internal energy.

The distributions of normalized static pressure at the same condition to Fig. 8 are presented in Fig. 9. The normalized static pressure is not peculiarly varied in conformity with the stagnation temperature change.

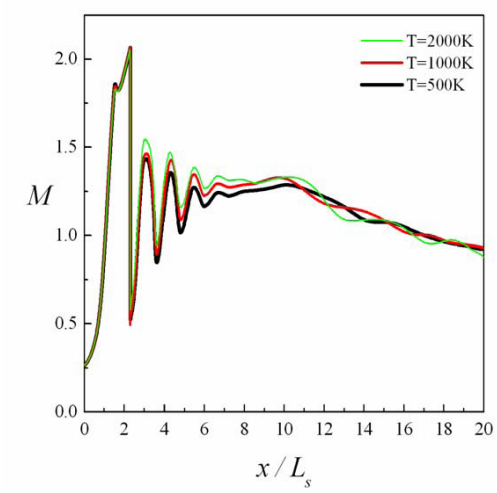

Fig. 8. Mach number distributions along the nozzle centerline according to the variation of stagnation temperature at NPR=3.413.

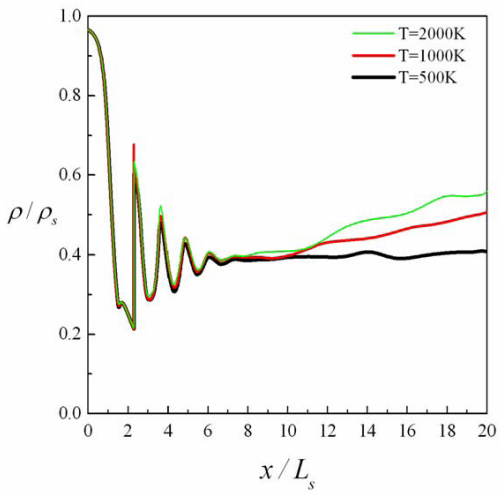

Fig. 10. Normalized density distributions along the nozzle centerline according to the variation of stagnation temperature at NPR=3.413.

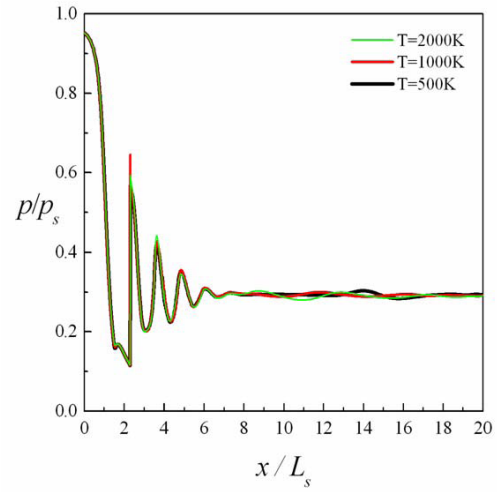

Fig. 9. Static pressure distributions along the nozzle centerline according to the variation of stagnation temperature at NPR=3.413.

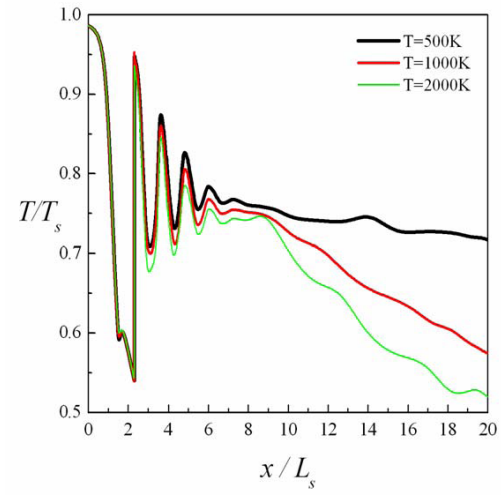

Fig. 11. Normalized temperature distributions along the nozzle centerline according to the variation of stagnation temperature at NPR=3.413.

Since pressure in the range of x/L_s>7 does not fluctuate severely, the variation of the stagnation temperature behaves itself under the nearly isobaric condition.

Fig. 10 depicts the normalized density distributions on the nozzle centerline when the stagnation temperature changes at the same NPR (3.413) to the above mentioned condition. As the entrance stagnation temperature is high, fluid density tends to increase in downstream of the thruster exit. This feature is related to the temperature distribution which can be explained as follows. It is found that $\rho T = const$ based on the equation of state because the pressure distribution is rarely affected by the stagnation temperature variation as shown in Fig. 9. Therefore, density and temperature are inversely proportional to each other. $\rho T/\rho_S T_S$ is approximately 0.28 in the range of x/L_s>7. Because temperature decreases as getting toward downstream, density increases gradually corresponding to temperature under the quasi-isobaric pressure condition.

Fig. 11 shows the normalized temperature distribu-

tions on the central axis of the nozzle when the stagnation temperatures at the nozzle entrance are different under the same stagnation pressure condition. The stagnation temperature of the nozzle entrance has hardly an effect on the temperature distributions in front of normal shock waves; however, temperature has a tendency to diminish at the section of shock cells as the entrance stagnation temperature increases. The reason is the same as the previous explanation for the density variation.

3. Conclusions

Two-dimensional supersonic micro De Laval Nozzle flows over various pressure ratios and stagnation temperatures are investigated computationally to verify the shock structure in the plume. The different types in the Mach number distribution make an appearance in downstream of the nozzle exit according to NPR; the cell-type structure becomes clearer as NPR increases. The supersonic flow in this nozzle can be classified into two types. When NPR belongs to the range in which a strong lambda shock wave exists, the plume structure does not show reiterative between the slip streams. That is, if the shock shape near the exit is the Mach reflection, the shock cell structure does not show in the plume. On the other hand, when NPR is in the range that oblique shock waves are crossed like the regular reflection, the shock cell structure appears in the plume.

Even when the stagnation temperature changes in the nozzle entrance, the distributions of pressure, Mach number, density and temperature are little affected upstream of shock waves. Especially, the pressure distributions behind shock waves are not considerably influenced by the entrance stagnation temperature variation; thus, the product of density and temperature is nearly constant far downstream from the exit.

Acknowledgment

This work was supported by the NURI project of the Ministry of Education, Korea in 2006.

Nomenclature

a : speed of sound
$C_{1\varepsilon}, C_{2\varepsilon}, C_{\mu}$: 1.42, 1.68, and 0.0845, respectively
e : internal energy
k : turbulent kinetic energy
L_S : length of the divergent part of the nozzle
M : Mach number
NPR : Nozzle pressure ratio, p_s / p_a
p : Static pressure
p_a : Ambient pressure
p_S : Stagnation pressure
q_i : Heat flux
R : Gas constant
$S = \left[2^{-1} \left(\partial u_j / \partial x_i + \partial u_i / \partial x_j \right)^2 \right]^{1/2}$
T : Absolute temperature
T_S : Stagnation temperature
u_i : Velocity component
x : Coordinate of the main flow direction
x_i : Coordinates
x_t : Distance between the nozzle entrance and the nozzle throat
y : Normal to the x axis

Greek symbols

$\alpha_k, \alpha_\varepsilon, \beta, \eta_o$: 1, 1.22, 0.012, and 4.38, respectively
ε : Dissipation rate of the turbulent kinetic energy
$\eta = Sk / \varepsilon$
μ : Absolute viscosity
μ_t : Eddy viscosity
$\mu_{eff} = \mu + \mu_t$
ρ : Fluid density
ρ_S : Stagnation density
ν : Kinematic viscosity
τ_{ij} : Viscous shear stress
τ_w : Wall shear stress

References

[1] G. K. Cooper, J. L. Jordan and W. J. Phares, Analysis tool for application to ground testing of highly under-expanded nozzles, *AIAA/SAE/ASME/ASEE 23rd Joint Propulsion Conference*, San Diego, California, June 29-July 2, AIAA Paper 87-2015, (1987).

[2] J. Y. Koo, The effects of injector nozzle geometry and operating pressure conditions on the transient fuel spray behavior, *KSME Int'l J.* 17 (4) (2003) 617-625.

[3] T. Aoki, Y. H. Kweon, Y. Miyazato, H. D. Kim and T. Setoguchi, An experimental study of the nozzle lip thickness effect on supersonic jet screech tones,

J. of Mechanical Science and Technology, 20 (4) (2006) 522-532.

[4] S. Y. Han, Effect of boundary layer swirl on supersonic jet instabilities and thrust, *KSME Int'l J.* 15 (5) (2001) 646-655.

[5] C. A. Hunter, Experimental, theoretical, and computational investigation of separated nozzle flows, *AIAA/ASME/SAE/ASEE 34th Joint Propulsion Conference & Exhibit*, Cleveland, Ohio, July 13-15, AIAA Paper 98-3107 (1988).

[6] S. D. Kwon, S. Kim, J. S. Kim and J. Choi, Computation of a two-dimensional nozzle flow with the variation of pressure and length ratios, *J. of the KSASS*, 35 (4) (2007) 281-286.

[7] FLUENT 6.1 User's Guide (2003) Fluent inc.